A free-standing reduced graphene oxide aerogel as supporting electrode in a fluorine-free Li2S8 catholyte Li-S battery

Journal of Power Sources 416 (2019) 111–117

Contents lists available at ScienceDirect

Journal of Power Sources

journal homepage: www.elsevier.com/locate/jpowsour

A free-standing reduced graphene oxide aerogel as supporting electrode in a fluorine-free Li_2S_8 catholyte Li-S battery

Carmen Cavallo[a,**], Marco Agostini[a,***], James P. Genders[b], Muhammad E. Abdelhamid[c], Aleksandar Matic[a,*]

[a] Department of Physics, Chalmers University of Technology, SE 412 96, Gothenburg, Sweden
[b] Department of Chemistry, University of Southampton, Southampton, SO171 BJ, UK
[c] CSIRO Mineral Resources, Research Way, Clayton, VIC, 3168, Australia

HIGHLIGHTS

- New synthetic route for free-standing reduced graphene oxide aerogel.
- Semi-liquid Li-S cells designed through fluorine-free electrolyte medium.
- Reduced graphene oxide aerogel stabilizing Li-S cells cyclability and capacity retention.

GRAPHICAL ABSTRACT

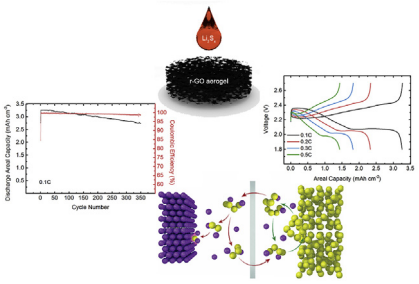

ARTICLE INFO

Keywords:
Li-S batteries
Energy storage
Reduced graphene oxide
Fluorine-free electrolyte for Li-S batteries
Polysulphide based catholyte electrodes

ABSTRACT

We report on a novel, simple, and environmentally benign synthesis route for a free-standing reduced graphene oxide (r-GO) aerogel and its application as supporting electrode for the electrochemical redox reaction of sulphur in a catholyte-based lithium-sulphur battery. A mesoporous matrix is formed by a layers of r-GO, providing sites for electrochemical reactions and a highly conducting pathway for electrons. The highly porous structure is easily infiltrated by a catholyte solution providing a homogeneous distribution of the sulphur active material in the conductive graphene matrix and ensuring efficient electrochemical reactions. This is demonstrated by a high capacity, 3.4 mAh cm^{-2}, at high mass loading, 3.2 mg cm^{-2} of sulphur in the cathode and in total the sulphur loading in the Li-S cell is even double (6.4 mg cm^{-2}). Additionally, the presence of oxygen groups in the r-GO aerogel structure stabilizes the cycling performance and the Li-S cell with the fluorine free catholyte shows a capacity retention of 85% after 350 cycles.

1. Introduction

Since its commercialisation in the early 1990s, most of the energy storage solutions for electronic devices have been based on Li-ion battery (LiBs) technology. However, Li-ion batteries have limited energy density and commercially available cells are approaching the energy density and materials availability limits [1–4]. The energy limit is set by the chemistry which is based on Li-ion insertion materials. Thus,

* Corresponding author.
** Corresponding author.
*** Corresponding author.
E-mail addresses: carmen.cavallo@chalmers.se (C. Cavallo), agostini@chalmers.se (M. Agostini), matic@chalmers.se (A. Matic).

https://doi.org/10.1016/j.jpowsour.2019.01.081
Received 18 October 2018; Received in revised form 20 December 2018; Accepted 27 January 2019
Available online 05 February 2019

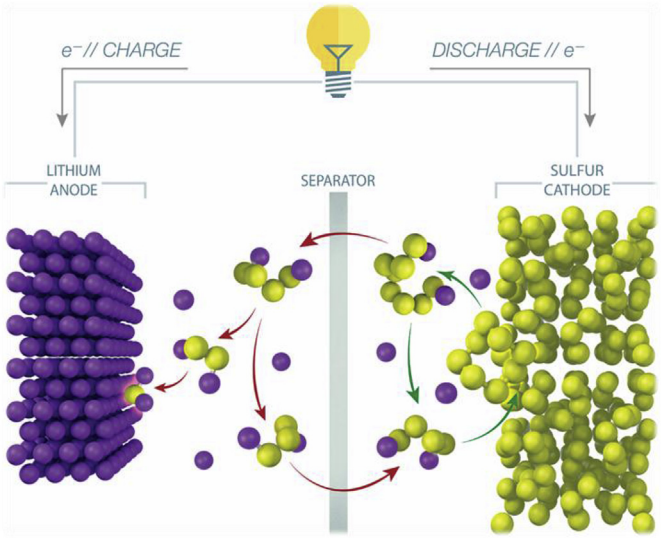

Fig. 1. Simplified schematic of the lithium-sulphur battery. Dissolution of polysulphide in the electrolyte (green arrows) and the undesirable shuttling mechanism (red arrows). (For interpretation of the references to colour in this figure legend, the reader is referred to the Web version of this article.)

to meet the demands of high-capacity applications, related to renewable energy sources, new chemistries, mostly based on conversion mechanism, need to be introduced to allow energy storage system to take a leap in energy density [5].

Sulphur, which is environmentally friendly, highly abundant, and cheap, offers a high theoretical specific energy density (2600 Wh/kg) and safe operating voltage (*ca.* 1.6–2.4 V vs. Li^+/Li) when combined with Li [6,7]. However, Li-S batteries suffer from different issues, so far limiting their development to a large scale commercial technology [8]. The main issue is the dissolution of the active material by the electrolyte and the following shuttling of polysulphides (Fig. 1) leading to a host of effects including increase in the resistivity of the solid electrolyte interface (SEI) due to deposition of insulating products on the Li-metal anode, active material loss and reduction in Coulombic efficiency. Altogether this results in low cycle life of the Li-S cell [9,10].

The formation of polysulphides and thus their presence in the cell is an intrinsic part of the electrochemical reaction (Equation (1)) [11]:

$$16Li^+ + S_8 + 16e^- \rightleftharpoons nLi_2S_x \rightleftharpoons 8Li_2S \quad (1)$$

In common electrolytes, based on organic solvents, the polysulphides formed, Li_2S_n n = 8-2, have a high to moderate solubility, whereas the end products S_8 and Li_2S have very low, or no solubility. The dissolution of Li-polysulphides in the electrolyte during cycling is a double-edged sword. In fact, a certain degree of dissolution is necessary for fast reaction kinetics (i.e. fast charging and discharging) and high active material utilization. However, once dissolved polysulphides tend to shuttle between the cathode and the anode due to the high concentration gradient in the electrolyte and electromotive forces [12,13]. Thus, rather than preventing polysulphide dissolution a path to stable cycling involves preventing continuous side reactions at the anode side and confining as large amount as possible of polysulphides in the cathode [14].

To stabilise the Li-metal anode and to prevent parasitic reactions several approaches have been proposed [15,16]. The most common is modifying the composition of the electrolyte, introducing for example sacrificial additives with the aim to form a stable interphase on the anode. The addition of $LiNO_3$ has been particularly common and shown to prevent the deposition of polysulphides on the anode side [17]. To buffer against migration of polysulphides from the cathode, Li_2S_n have been deliberately introduced in the electrolyte [18]. In addition to the buffering effect the presence of polysulphides has also been shown to contribute to electrochemical process with Li [19,20] and to the formation of a stable interphase on the Li-metal anode [21,22]. A further step in this direction is to have all the active material dissolved in the electrolyte, forming then a "catholyte", with the solid cathode only supporting the electrochemical reactions and acting as a conducting matrix in a semi-liquid cell [20–22]. Recently, a new approach was reported considering that the dissolved polysulphides can have dual roles, providing both the active material and Li-conduction in the electrolyte since they are in fact a Li-salt [23–25].

In order to fully utilise the active material (polysulphides) in cells with semi-liquid electrodes, a conductive matrix with high porosity is required. Different types of materials have been proposed being able to support the electrochemical reaction with Li, in particular, self-supporting carbon matrices, which do not require the addition of polymer binders or the use of the Al-current collector. Combined with high active material loading through the catholyte, high practical areal capacities (mAh cm^{-2}) and energy densities have been demonstrated (Wh kg^{-1}) [25–28]. Among the possible self-standing and binder free matrices, graphene-based materials have attracted considerable attention due to a high electronic conductivity and the possibility to synthesize highly porous structures [29–31]. However, applications in commercial devices are often limited by complex processing and high cost of synthesis when graphene is involved [32]. Graphene oxide (GO) offers instead a viable route for graphene based functional bulk materials with prospect for lower cost and bulk quantities. In its conductive reduced form (r-GO), it can be dispersed in many polar solvents including water [33], easily modified with functional groups at the surface and be used in Li-S batteries systems [34–36].

In this work, we report on a novel strategy for the synthesis of an ultralow-density, free-standing and porous r-GO aerogel and its application as support in semi-liquid Li-S cells. The interconnection of the 3D conductive framework of the r-GO aerogels with the presence of pores and a high conductive path facilitate the reaction of Li^+ with polysulphides, while the presence of oxygen polar groups reduces Li_2S_n migration to the anode and stabilizes the capacity of the Li-S cells for more than 350 cycles. Furthermore, the combination of the graphene aerogel with a fluorine-free catholyte solution, where the added polysulphide acts also as conducting agent, avoids the presence of traditional Li-salts based on fluorine species, such as $LiN(SO_2CF3)_2$ or $LiCF_3SO_3$ and enable LiS-cells with high practical capacity.

2. Experimental

2.1. Synthesis of 3D reduced graphene oxide aerogel and Li_2S_8 catholyte

All chemicals were of analytical grade and used as received. The GO dispersion (4 mg/mL, 95% monolayer) was purchased from Graphenea (Germany). L-Ascorbic acid, hydrochloric acid (HCl), Sulphur, lithium sulphide (Li_2S), lithium nitrate ($LiNO_3$), 1,3-Dioxolane (DOL), and 1,2-Dimethoxyethane (DME) were purchased from Sigma Aldrich.

The synthesis procedure of the r-GO aerogel is illustrated in Fig. 2. 10 g of GO suspension (4 mg/mL) was sonicated with a probe sonicator (Qsonica XL-2000-010 Microson XL2000, 220 VAC), keep controlling the temperature of the suspension at 25 °C and then loaded in a 40 mL vial. Subsequently the suspension was added to a reducing solution, 80 mg of L-ascorbic acid 100 µL of HCl 5 mol L^{-1} in 30 mL of distilled water. The reason for choosing L-ascorbic acid as the reducing agent is the lack of gaseous by-products during the formation of the gel precursor which is of importance in order to obtain a homogeneous gel.

When using traditional reducing agents, such as hydrazine, $NaBH_4$ or $LiAlH_4$, non-uniform gels are formed due to the evolution of gaseous by-products [37]. The postulated reduction mechanism with L-ascorbic acid is a two-step S_N2 nucleophilic reaction followed by a one-step thermal elimination and HCl was added in order to catalyse the reaction. The GO suspension/L-ascorbic acid mixture was sonicated for at least half hour and then heated at 90 °C for at least 8 h. After gelation,

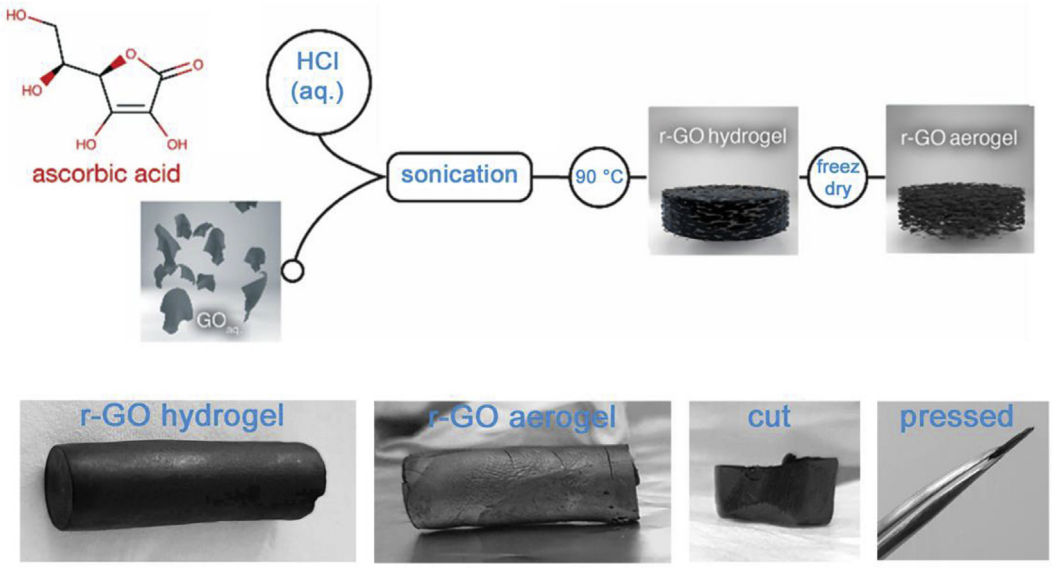

Fig. 2. Scheme of the synthesis of the r-GO aerogel and photographs of final synthetic steps. The proposed self-assembled reaction scheme catalysed by HCl (5 m L^{-1}), between L-ascorbic acid (80 mg) and aqueous GO suspension (4 m L^{-1}). Sonication, heating (90 °C) and freeze-dry processes, necessary to complete the synthesis of the r-GO aerogel. Photographs of r-GO hydrogel, r-GO aerogel, cut and pressed r-GO aerogel disc are presented.

the wet r-GO gel was immersed in deionized water to remove any impurities and unreacted GO sheets. Subsequently, the hydrogel was carefully frozen in a closed container with liquid nitrogen and transferred into a freeze dryer in order to preserve the original porosity and prevent the collapse of the r-GO aerogel structure (see the photographs in Fig. 2). After being pressed, the rGO disk shows a good mechanical stability and can directly be assembled in the coin cell. In order to obtain a stable aerogel, we have optimized the process by using a lower concentration of L-ascorbic acid, 0.01 M, and a higher temperature, 90 °C. The main point with these processing conditions was to slow down the reduction process. At higher concentration of ascorbic acid the process is too fast resulting in the formation of a rGO flakes in the suspension preventing the formation of an aerogel.

The Li_2S_8–catholyte solution (final concentration 0.5 mol L^{-1}) was prepared by mixing Li_2S and sulphur in a 1:7 M ratio in DME (Dimethoxyethane)/DOL (Dioxolane) with a 1:1 vol ratio at room temperature and stirring the solution for 24 h. Subsequently, 0.4 mol $L^{-1}$of $LiNO_3$ was added to the DOL-DME 0.5 mol L^{-1} Li_2S_8 solution and stirred for 24 h.

2.2. Materials characterization

X-ray diffraction (XRD) analysis was performed using a X'Pert Pro diffractometer (Cu Kα radiation, λ = 0.154184 nm) equipped with an X'Celerator ultrafast RTMS detector. The angular range was 10–90° (in 2θ). Raman spectrum was collected by means of a Labram Raman spectrometer, 514 nm excitation wavelength. The morphology of the r-GO aerogel was investigated using a Zeiss He Ion Microscope (HIM) – ORION (30 kV He ion beam) with a probe size < 0.5 nm for high resolution imaging [38,39] and a monochromated and double aberration-corrected (CETCOR image and ASCOR probe Cs-correctors) TEM JEOL-ARM (200 kV) 40-200 equipped with a field emission gun (FEG). The reduction of GO in r-GO was investigated by EDS (Energy Dispersive Spectroscopy) analysis on a JSM 7800F scanning electron microscope. N_2 adsorption and desorption isotherms were recorded at 196 °C using a Micromeritics Tristar instrument. The pore volume and size distribution were determined from the adsorption curve by the BJH (Barret-Joyner-Halenda) method and the specific surface area was calculated by the BET (Brunauer Emmet and Teller) multipoint method. All characterization was performed on pressed aerogel discs, see Fig. 2, in order to have the same geometry and configuration as in the assembled Li-S cells.

2.3. Electrochemical analysis and battery testing

The aerogels were electrochemically tested as conductive support in Li-S cells. Discs of r-GO aerogel (~10 mm diameter) were easily cut and pressed at 1000 psi pressure. The thickness of the disc after pressing was of about 300 μm while before pressing it was around 1 mm. The weight of the disc per cm^2 was of 0.23 mg cm^{-2}. The pressed discs were transferred to a glove box (H_2O and O_2 less than 1 ppm) and dried under vacuum at 80 °C in a Buchi oven. Coin cells were assembled in an argon-filled glovebox using CR2032 housings. The dried pressed aerogel discs were placed directly in the coin cell without the use of metal current collectors. Celgard® 2400 was used as separator, soaked with 20 μL of catholyte solution while lithium metal disc was used as anode (ϕ = 11 mm, 4 mg cm^{-2}). Further 20 μL of the catholyte solution, was added to the aerogel disc, corresponding to a sulphur loading of 3.26 mg cm^{-2} in the aerogel, calculated to totally fill the pores of the aerogel. Higher sulphur loading, i.e. larger volume of catholyte added to the aerogel, can not be absorbed and would be part of the electrolyte (in the separator), and not participating in the electrochemical reaction. The weight ratio between the sulphur loaded in the r-GO and the r-GO is S/r-GO = 12.5. The 3.26 mg cm^{-2} value was used for calculating the current density (mA cm^{-2}) of the Li-S cells. The overall sulphur loading in the Li-S cell was of 6.52 mg cm^{-2} considering also the catholyte added to the separator. The electrochemical cycling tests were performed between 1.8 V and 2.6 V using a current rate of 0.1 C (1C = 1675 mA g^{-1}, or 5.4 mA cm^{-2} considering a mass loading of 3.3 mg cm^{-2}) using a Scribner 580 battery cycler. When going from charge to discharge, the instrument records a first point at value lower than what is related to the electrochemical process, i.e. the open circuit voltage of the tested cell. For the rate capability analysis current rates of 0.1C, 0.2C, 0.3C and 0.5C were applied for 5 cycles each where after the current rate was lowered back to 0.1C.

3. Results and discussion

Following our new synthesis scheme outlined in Fig. 2 we obtained freestanding r-GO aerogels with a density of 7.7 mg cm^{-3}, which falls in

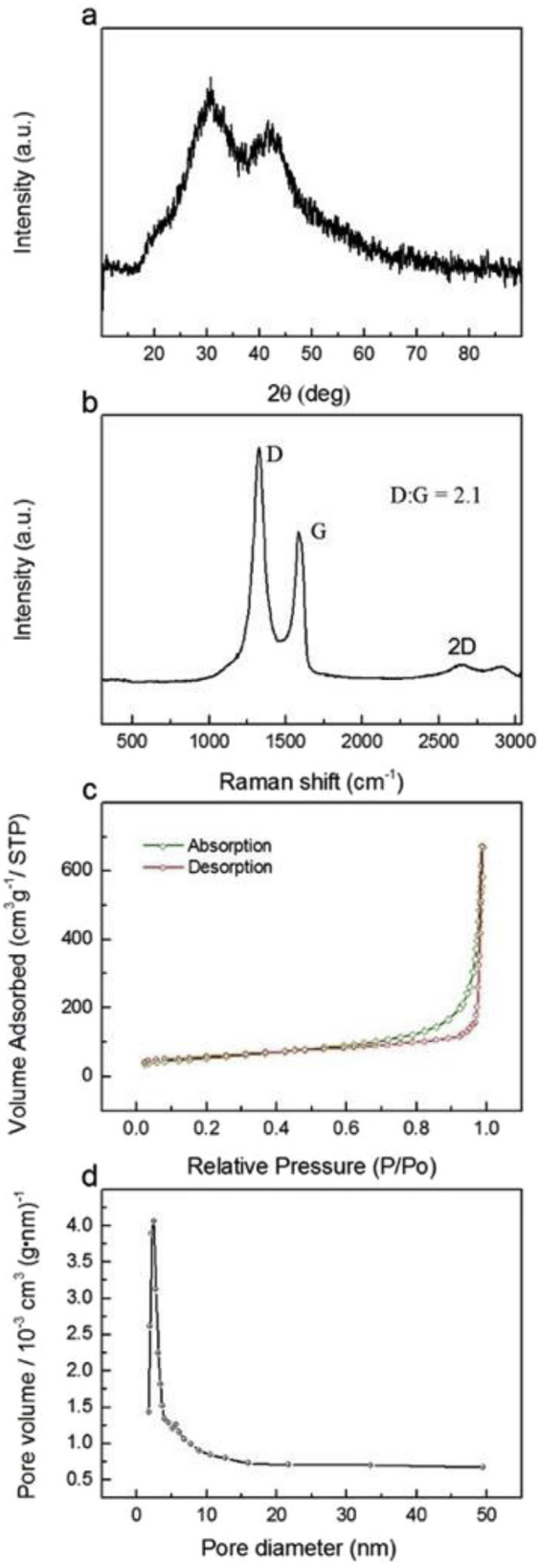

Fig. 3. Characterization of the 3D r-GO aerogel. a X-Ray diffraction pattern of the aerogel. **b** Raman spectra showing the characteristic D (~1350 cm^{-1}), G (~1580 cm^{-1}) peaks and the broad 2D band (from 2681 to 3959 cm^{-1}). **c** Nitrogen absorption desorption isotherms. **d**. Pore size distribution as determined from BJH measurement.

the range of ultralow-density materials [40]. The successful reduction of the graphene oxide during the synthesis procedure is confirmed by XRD analysis, Raman spectroscopy and EDS analysis. In the XRD pattern of the r-GO aerogel, see Fig. 3a, the contribution in the diffraction pattern between 20° and 50° 2Θ is ascribed to stacked planes of rGO and is commonly found in amorphous carbon [41].

Additionally, the disappearance of the characteristic peak of GO at $2\theta = 11°$ and the observation of two broad diffraction peaks ($2\theta \sim 30°$ and 45°) further confirms the effective reduction of GO by L-ascorbic acid. The broad peak at $2\theta \sim 30°$ is close to the (002) diffraction peak of graphite (d-spacing 3.35 Å at $2\theta = 27°$), whereas the peak at $2\theta \sim 43°$, indicates short-range order of stacked graphene layers [42].

In the Raman spectrum of the r-GO aerogel (Fig. 3b) the characteristic D, G, and 2D bands are observed. Typically, Raman spectra of a pristine GO shows an intensity ratio between the D and G bands around 0.9, indicating the presence of defects in the crystal lattice [43]. Upon chemical reduction of GO, an increase in the D/G ratio is usually observed [44]. The Raman spectra of our r-GO aerogels (Fig. 3b) reveals that the ratio between D and G bands is ~2.1.

The enhanced intensity of the D band, as well as the 2D band, is a sign of the presence of a large number of defects, resulting from the high frequency ultra-sonication treatment during the synthesis which causes graphene sheets to break into smaller flakes and produces defects [45].

The morphology of the material, in particular in terms of pores size and distribution, is a key property when designing supports for semi-liquid Li-S cells. Nitrogen adsorption/desorption measurements, reported in Fig. 3c–d, show that the r-GO aerogel has a surface area of 188 ± 2 m^2/g and that it is mesoporous with the majority of the pores being in the range of 2–10 nm. This is important considering that Li-sulphide species are formed *in situ* upon discharge/charge electrochemical process and that small the pores prevents the formation of large sulphur/sulphide aggregates which would slow down the kinetics and reduce the efficiency of the electrochemical reactions. Fig. 4 shows He-ion microscope (HIM) images of the morphology of the r-GO aerogel. Comparing the images from lowest to highest magnification we find a hierarchical 3D network structure with large voids ranging from 10 micrometres down to 100 nm, formed by layers of cross-linked graphene. Fig. 4c–d show different thicknesses of the r-GO layers, where dark areas indicate a thick stacking while lighter areas indicate a thinner stacking of the graphene sheets. In Fig. 4e a SEM image and an EDS map are shown. They reveal the presence of oxygen in the r-GO aerogel network with a C:O atomic ratio of ~88:12. The presence of oxygen makes the surface of the aerogel polar and provides sites for interaction for polysulphides which contributes to reduce the shuttle mechanism [46].

The structure and morphology of the r-GO aerogel is further investigated by the transmission electron microscopy analysis (TEM) (Fig. S1 in supporting information section (SI)). The images show the presence of stacked graphene layers at the edge of the aerogel, while in the interior we find thinner walls with e.g. 6 sheets as in Fig. S1c.

To evaluate the 3D r-GO aerogel as support in a semi-liquid LiS-cell, prolonged electrochemical tests were performed in a full LiS-cell configuration. Fig. 5a reports the cell design and this cell configuration has the advantage of not using a metal current collector, such as Aluminium or Copper foil, since the r-GO is used directly for the electrochemical redox reaction of the Li-polysulphides as a binder free and self-standing conductive matrix. Furthermore, in the catholyte solution there is no addition of conventional Li-salts, such as $LiN(SO_2CF_3)_2$ or $LiCF_3SO_3$, since the Li_2S_n polysulphides in the electrolyte soaked Celgard separator ensures Li-ion mobility [23–25]. The small amount of $LiNO_3$ (0.4 mol L^{-1}) reduces the effect of both the shuttle mechanism and the deposition of polysulphides on the anode thanks to the formation of a stable solid electrolyte interface (SEI) layer [15,47].

The electrochemical reaction mechanism of our Li-S cell based on Li_2S_8 catholyte reaction can be understood by analysing the discharge/

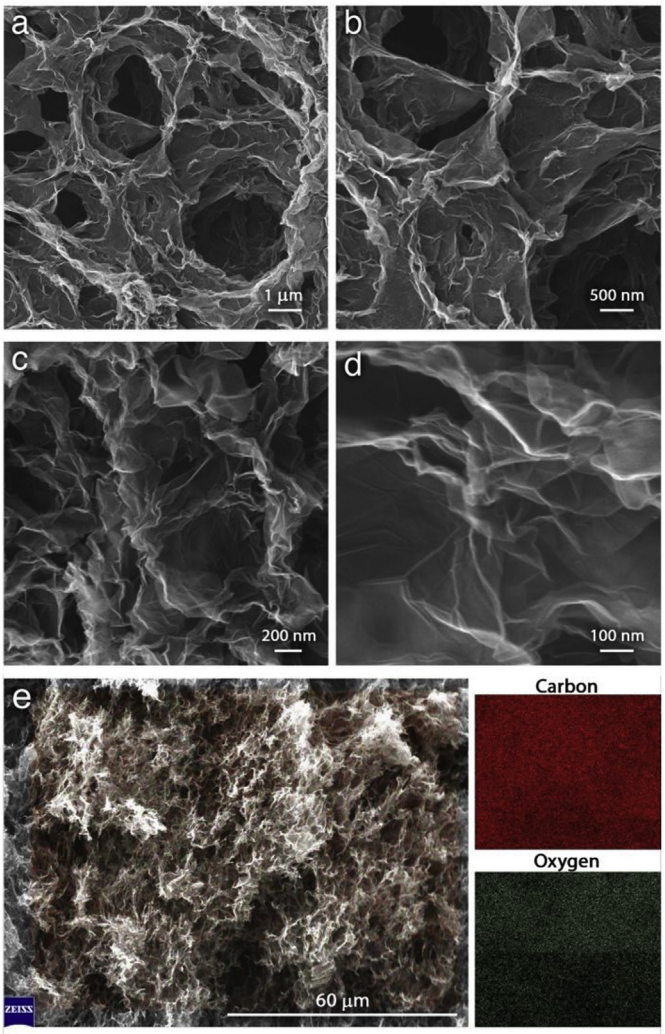

Fig. 4. Morphological investigation of the 3D r-GO. Helium Ion Microscopy images of r-GO aerogels with increased magnification from **a** to **d**. Scanning electron microscopies at different magnification (**a** to **e**) and Energy Dispersive Spectroscopy (EDS) mapping of Carbon (red) and Oxygen (green). (For interpretation of the references to colour in this figure legend, the reader is referred to the Web version of this article.)

charge curve. During the 1st discharge only 1 plateau, around 2.1 V, can be observed whereas in the subsequent cycles 2 plateaus are found, at 2.4V and 2.1V respectively, Fig. 5b.

This is a consequence of the fact that the first discharge starts from the conversion of Li_2S_8 to lower chain polysulphides and the plateau at 2.4V related to the conversion of S_8 to Li_2S_8 is then absent [20,25]. In the subsequent 1st charge there is a full reduction to S_8 and consequently in the 2nd discharge the capacity increases and we observe the characteristic profile with two voltage plateaus that corresponding to the full conversion from S to Li_2S according to eq. (1). Thus, the r-GO aerogel is able to fully support the conversion reaction with a high efficiency from the second cycle.

The cycling performance of the cell is reported in Fig. 6a. The cell delivers an initial areal capacity of 3.25 mAh cm^{-2} and 2.8 mAh cm^{-2} after 350 cycles at a current rate of 0.1C (0.54 mA cm^{-2}). Thus, the capacity retention is 86% over 350 cycles and at the same time the coulombic efficiency is 99.5% over full cycling test. The voltage profile of the Li-S cell at 50th, 100th, 200th and 350th cycle is shown in Fig. 6b and highlights that the discharge process corresponds to the typical one for Li-S reaction in DOL/DME solvent, as discussed above, with an overall working voltage of about 2.1V.

Rate capability tests were performed to further investigate the response of the r-GO aerogel/catholyte cell at higher current rates and the capacity retention with respect to rate, Fig. 6 c and d. The test starts at 0.1C (0.54 mA cm^{-2}) and the current rate is increased in 4 steps to 0.5C (2.7 mA cm^{-2}). With increasing current rate the voltage polarisation increases, which can be ascribed to the ohmic drop at higher current related to both the conductivity of the electrolyte and the conductivity of the r-GO aerogel. At the lowest current rate the Li-S cell delivers 3.25 mAh cm^{-2} while, when the current is increased 4 times, the cell still delivers a capacity around 1.5 mAh cm^{-2}. The flat plateau at higher rate is shortened as a consequence of reaction kinetics, i.e. a reduced amount of polysulphides in the catholyte solution has time to react leading to a lower active materials utilization. Furthermore, when the current rate is lowered back to the initial value of 0.1C, the Li-S cell recovers almost 96% of the initial capacity, showing an excellent retention with respect to increased current rate.

The performance of the here designed semi-liquid Li-S cell is mainly due to the beneficial morphology of the r-GO aerogel allowing for a large uptake of the catholyte and the mesoporous structure that enables efficient electrochemical reactions with fast kinetics [19–21]. Our new synthesis route, using a mild reducing agent, also ensures a homogeneous structure with strong cross-links preventing mechanical failure during cell assembly and cycling, and thus enables long cycle life. The oxygens at the surface of the r-GO aerogel act as interaction points for

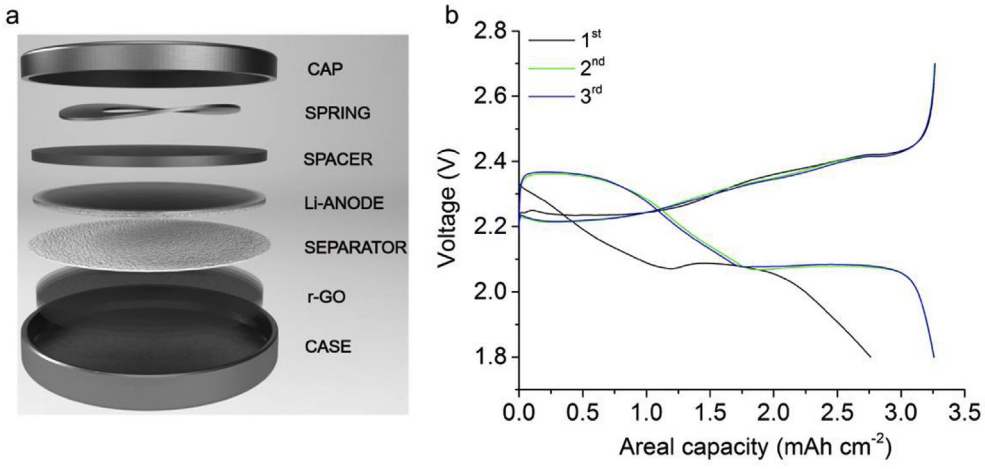

Fig. 5. Configuration of the catholyte LiS-cell using r-GO aerogel and electrochemical mechanism. a The 3D r-GO aerogel is directly cut and seated on the case of the cell without any current collector. **b** Voltage profiles during the 1st, 2nd and 3rd cycle of the Li-S semi liquid cell.

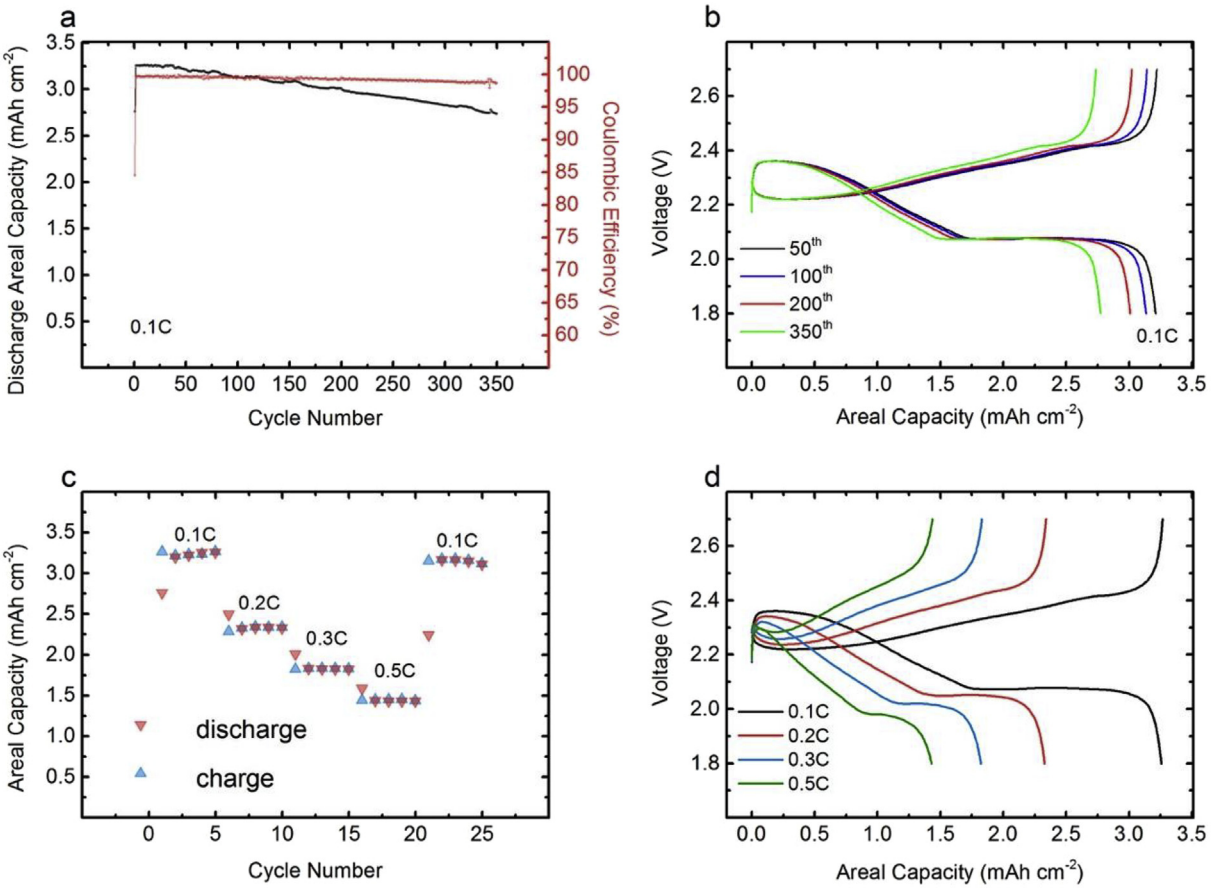

Fig. 6. Cycling performance of the Li/S catholyte-based cell with the r-GO aerogel as support. a Prolonged cycling performance in lithium half-cell configuration at 0.1C (0.54 mA cm^{-2}, black dots) and corresponding Columbic efficiency (red dots). **b** Galvanostatic voltage profile at the 50^{th}, 100^{th}, 200^{th} and 350^{th} cycle. **c** Rate capability measurements at different current rate (from 0.1C to 0.5C) and **d** corresponding voltage profiles. (For interpretation of the references to colour in this figure legend, the reader is referred to the Web version of this article.)

the polysulphides and reduces the shuttle mechanism and the following deposition on Li metal anode together with the dissolved $LiNO_3$ salt. Moreover, the presence of dissolved polysulphides in the electrolyte, provides both Li^+ conduction and also buffer the migration of polysulphide species from the mesopores of the r-GO support. These combined effects lead to a superior performance in areal capacity and cycling stability of the r-GO/catholyte Li-S cell.

4. Conclusions

3D r-GO aerogels were synthesised and used as electrode support for a catholyte-based Li-S cell. The new ultralow density r-GO aerogels were prepared *via* a novel synthesis route based on the reduction of a solution of graphene oxide by L-ascorbic acid catalysed by HCl. We show that the self-standing r-GO aerogel can be successfully applied as support for the redox process of a fluorine-free Li-polysulphide catholyte in a Li-S cell. In catholyte based systems, a matrix that is not self-standing and not-functionalized is normally used to support the electrochemical reaction of the sulphur [18–21]. Despite of the delivered capacity could result high, it is however limited by the low concentration of the catholyte and thus by the low sulphur weight. These limits are given by the not optimized porosity and pores size of the matrix supporting the electrochemical reaction, as well as by its design. Indeed, we show that the presence of functional groups at the surface of the counter electrode, i.e. oxygen, is mandatory to achieve high utilization of the polysulphides species and reduced shuttle effect, together with a tailored porosity, pores size and surface area [25,46]. The here designed aerogel has a mesoporous morphology, with presence of oxygen groups at the surface, resulting in fast kinetics and reduced shuttle reactions. The r-GO aerogel/catholyte cell demonstrates a high areal capacity, up to 3.4 mAh cm^{-2}, and extended cycle-life, more than 350 cycles with 85% capacity retention. The presence of Li_2S_n in the electrolyte not only guarantees the conduction of Li^+ ions but also buffers Li-polysulphide migration from the cathode. By employing low cost and environmental friendly materials, such as carbon and sulphur, and avoiding the use of expensive fluorine-based Li-salts, we demonstrated the possibility to develop advanced Li-S batteries with high areal capacity.

Acknowledgments

The authors would like to thank ZEISS for the HIM measurements, in particular Dr. Jens Wigenius and Dr. Peter Gnauck. The authors acknowledge the support from the Chalmers Areas of Advance Materials Science and Energy, the Swedish Energy Agency and the access to microscopy facilities of Chalmers Materials Analysis Laboratory (CMAL, in particular Dr. Reza Zamani).

Appendix A. Supplementary data

Supplementary data to this article can be found online at https://doi.org/10.1016/j.jpowsour.2019.01.081.

References

[1] G. Crabtree, E. Kocs, L. Trahey, The energy storage frontier: lithium-ion batteries

and beyond, MRS Bull. 40 (2015) 1067–1078 https://doi.org/10.1557/mrs.2015.259.
[2] R.C. Armstrong, et al., The frontiers of energy, Nature En 1 (2016) 15020 https://doi:10.1038/nenergy.2015.20.
[3] S. Chu, Y. Cui, N. Liu, The path towards sustainable energy, Nat. Mater. 16 (2017) 16–22 https://doi:10.1038/nmat4834.
[4] J. Janek, W.G. Zeier, A solid future for battery development, Nat. Energy 500 (2016) 300 16141 https://doi.org/10.1038/nenergy.2016.141.
[5] B. Scrosati, J. Garche, Lithium batteries: status, prospects and future, J. Power Sources 195 (2010) 2419–2430 https://doi:10.1016/j.jpowsour.2009.11.048.
[6] A. Manthiram, Y. Fu, Y.S. Su, Challenges and prospects of lithium-sulfur batteries, Acc. Chem. Res. 46 (2013) 1125–1134 https://doi:10.1021/ar300179v.
[7] L. Chen, L.L. Shaw, Recent advances in lithium-sulfur batteries, J. Power Sources 267 (2014) 770–783 https://doi:10.1016/j.jpowsour.2014.05.111.
[8] B. Scrosati, J. Hassoun, Y.-K. Sun, Lithium-ion batteries. A look into the future, Energy Environ. Sci. 4 (2011) 3287–3295 https://doi:10.1039/C1EE01388B.
[9] X. Yu, A. Manthiram, A class of polysulfide catholytes for lithium-sulfur batteries: energy density, cyclability, and voltage enhancement, Phys. Chem. Chem. Phys. 17 (2015) 2127–2136 https://doi:10.1039/C4CP04895D.
[10] A. Manthiram, Y. Fu, S.H. Chung, C. Zu, Y.S. Su, Rechargeable lithium-sulfur batteries, Chem. Rev. 114 (2014) 11751–11787 https://doi:10.1021/cr500062v.
[11] R.D. Rauh, K.M. Abraham, G.F. Pearson, J.K. Surprenant, S.B. Brummer, A lithium/dissolved ulfur battery with an organic electrolyte, J. Electrochem. Soc. 126 (1978) 523–527 https://doi:10.1149/1.2129079.
[12] M. Barghamadi, A.S. Best, A.I. Bhatt, A.F. Hollenkamp, M. Musameh, R.J. Rees, T. Rüther, Lithium-sulfur-batteries-the solution is in the electrolyte, but is the electrolyte a solution, Energy Environ. Sci. 7 (2014) 3902–3920 https://doi:10.1039/C4EE02192D.
[13] S. Xiong, K. Xie, E. Blomberg, P. Jacobsson, A. Matic, Analysis of the solid electrolyte interphase formed with an ionic liquid electrolyte for lithium-sulfur batteries, J. Power Sources 252 (2014) 150–155 https://doi:10.1016/j.jpowsour.2013.11.119.
[14] M. Agostini, B. Scrosati, J. Hassoun, An advanced lithium-ion sulfur battery for high energy storage, Adv. Energy Mater. 5 (2015) 1500481 https://doi.org:/10.1002/aenm.201500481.
[15] D. Aurbach, E. Pollak, R. Elazari, G. Salitra, C.S. Kelley, J. Affinito, On the surface chemical aspects of very high energy density, rechargeable Li-sulfur batteries, J. Electrochem. Soc. 156 (2009) A694–A702 https://doi:10.1149/1.3148721.
[16] R. Kumar, J. Liu, J.-Y. Hwang, Y.-K. Sun, Recent research trends in Li-S batteries, J. Mater. Chem. A 6 (2018) 11582–11605 https://doi:10.1039/c8ta01483c.
[17] S. Xiong, K. Xie, Y. Diao, X. Hong, Properties of surface film on lithium anode with LiNO3 as lithium salt in electrolyte solution for lithium-sulfur batteries, Electrochim. Acta 83 (2012) 78–86 https://doi.org/10.1016/j.electacta.2012.07.118.
[18] D.-J. Lee, M. Agostini, J.-W. Park, Y.-K. Sun, J. Hassoun, B. Scrosati, Progress in lithium-sulfur batteries: the effective role of a polysulfide-added electrolyte as buffer to prevent cathode dissolution, ChemSusChem 6 (2013) 2245–2248 https://doi.org/10.1002/cssc.201300313.
[19] Y. Yang, G. Zheng, Y. Cui, A membrane-free lithium/polysulfide semi-liquid battery for large-scale energy storage, Energy Environ. Sci. 6 (2013) 1552–1558 https://doi:10.1039/C3EE00072A.
[20] M. Agostini, D.J. Lee, B. Scrosati, Y.-K. Sun, J. Hassoun, Characteristics of Li2S8-tetraglyme catholyte in a semi-liquid lithium-sulfur battery, J. Power Sources 265 (2014) 14–19 https://doi:10.1016/j.jpowsour.2014.04.074.
[21] M. Agostini, S. Xiong, A. Matic, J. Hassoun, Polysulfide-containing glyme-based electrolytes for lithium-sulfur battery, Chem. Mater. 27 (2015) 4604–4611 https://doi.org/10.1021/acs.chemmater.5b00896.
[22] S. Xiong, K. Xie, Y. Diao, X. Hong, On the role of polysulfides for a stable solid electrolyte interphase on the lithium anode cycled in lithium-sulfur batteries, J. Power Sources 236 (2013) 181–187 https://doi:10.1016/j.jpowsour.2013.02.072.
[23] R. Xu, I. Belharouak, J.C.M. Li, X. Zhang, I. Bloom, J. Bareño, Role of polysulfidde in self-healing lithium-sulfur batteries, Adv. Energy Mater. 3 (2013) 833–838 https://doi.org/10.1002/aenm.201200990.
[24] M. Agostini, D.H. Lim, M. Sadd, J.-Y. Hwang, S. Brutti, J. Heo, J. Ahn, Y.-K. Sun, A. Matic, Rational design of low cost and high energy lithium batteries through tailored fluorine-free electrolyte and nanostructured S/C composite, ChemSusChem 25 (2018) 2981–2986 https://doi.org/10.1002/cssc.201801017.
[25] D.H. Lim, M. Agostini, F. Nitze, J. Manuel, J.H. Ahn, A. Matic, Route to sustainable lithium-sulfur batteries with high practical capacity through a fluorine free polysulfide catholyte and self-standing Carbon Nanofiber membrane, Sci. Rep. 7 (2017) 6327 https://doi.org/10.1038/s41598-017-06593-2.
[26] P. Xiong, G. Yang, C. Yu, Liquid-type cathode enabled by 3D sponge-like carbon nanotubes for high energy density and long cycling life of Li-S batteries, Adv. Mater. 26 (2014) 7456–7461 https://doi.org/10.1002/adma.201403337.
[27] H. Pan, et al., Non-encapsulation approach for high-performance Li–S batteries through controlled nucleation and growth, Nat. Energy 2 (2017) 813–820 https://doi.org/10.1038/s41560-017-0005-z.
[28] Y.-K. Sun, C.S. Yoon, Growing instead of confining, Nat. Energy 2 (2017) 768–769 https://doi.org/10.1038/s41560-017-0008-9.
[29] G. Gorgolis, C. Galiotis, Graphene aerogels: a review, 2D Mater. 4 (2017) 032001 https://doi.org/10.1088/2053-1583/aa7883.
[30] R. Racicchini, A. Varzi, S. Passerini, B. Scrosati, The role of graphene for electrochemical energy storage, Nat. Mater. 14 (2015) 271–279 https://doi.org/10.1038/nmat4170.
[31] F. Nitze, M. Agostini, F. Lundin, A.E. Palmqvist, A. Matic, A binder-free sulfur/reduced graphene oxide aerogel as high performance electrode materials for lithium sulfur batteries, Sci. Rep. 6 (2016) 39615 https://doi:10.1038/srep39615.
[32] L. Grande, V.T. Chundi, D. Wei, C. Bower, P. Andrew, T. Ryhänen, Graphene for energy harvesting/storage devices and printed electronics, Particuology 10 (2012) 1–8 https://doi:10.1016/j.partic.2011.12.001.
[33] Z.Y. Xia, et al., The exfoliation of graphene in liquids by electrochemical, chemical, and sonication-assisted techniques: a nanoscale study, Adv. Funct. Mat. 23 (2013) 4684–4693 https://doi.org/10.1002/adfm.201203686.
[34] O.C. Compton, T.S. Nguyen, Graphene oxide, highly reduced graphene oxide, and graphene: versatile building blocks for carbon-based materials, Small 6 (2010) 711–723 https://doi:10.1002/smll.200901934.
[35] S. Stankovich, D.A. Dikin, G.H.B. Dommett, K.M. Kohlhaas, E.J. Zimney, E.A. Stach, R.D. Piner, S.T. Nguyen, R.S. Ruoff, Graphene-based composite materials, Nature 442 (2006) 282–286 https://doi:10.1038/nature04969.
[36] J. Song, Z. Yu, M.L. Gordin, D. Wang, Advanced sulfur cathode enabled by highly crumpled nitrogen-doped graphene sheets for high-energy-density lithium-sulfur batteries, Nano Lett. 16 (2016) 864–870 https://doi:10.1021/acs.nanolett.5b03217.
[37] C.K. Chua, M. Pumera, The reduction of graphene oxide with hydrazine: elucidating its reductive capability based on a reaction-model approach, Chem. Commun. 52 (2016) 72–75 https://doi:10.1039/C5CC08170J.
[38] L. Scipioni, L.A. Stern, J. Notte, S. Sijbrandij, B. Griffin, Helium ion microscope, Adv. Mater. Process. 166 (2008) 27–30.
[39] J. Morgan, J. Notte, R. Hill, B. Ward, An introduction to the helium ion, Microsc. Today 14 (2006) 24–31.
[40] A.J. Jacobsen, T.A. Schaedler, W.B. Carter, Ultralow-density Materials: from Aerogels to Microlattices, McGraw-Hill Education, 2013, https://doi.org/10.1036/1097-8542.YB13104.
[41] Y. Wang, J. Liu, L. Liu, D.D. Sun, High-quality reduced graphene oxide-nanocrystalline platinum hybrid materials prepared by simultaneous co-reduction of graphene oxide and chloroplatinic acid, Nanoscale Res. Lett. 6 (1–8) (2011) 241 https://doi.org/10.1186/1556-276X-6-241.
[42] B. Lesiak, L. Stobinski, A. Malolepszy, M. Mazurkiewicz, L. Kövér, J. Tóth, Preparation of graphene oxide and characterisation using electron spectroscopy, J. Electron Spectrosc. 193 (2014) 92–99 https://doi:10.1016/j.elspec.2014.03.015.
[43] C.K. Chua, Z. Sofer, M. Pumera, Graphite oxides: effects of permanganate and chlorate oxidants on the oxygen composition, Chemistry 18 (2012) 13453–13459 https://doi:10.1002/chem.201202320.
[44] W. Gao, Graphene Oxide. Reduction Recipes, Spectroscopy and Applications, Springer, 2015, pp. 61–95.
[45] J. Hassoun, et al., An advanced lithium-ion battery based on a graphene anode and a lithium iron phosphate cathode, Nano Lett. 14 (2014) 4901–4906 https://doi:10.1021/nl502429m.
[46] M. Agostini, J.-Y. Hwang, H.M. Kim, P. Bruni, S. Brutti, F. Croce, A. Matic, Y.-K. Sun, Minimizing the electrolyte volume in Li–S batteries: a step forward to high gravimetric energy density, Adv. Energy Mater. 8 (2018) 1801560 https://doi.org/10.1002/aenm.201801560.
[47] W. Li, H. Yao, K. Yan, G. Zheng, Z. Liang, Y.-M. Chiang, Y. Cui, The synergetic effect of lithium polysulfide and lithium nitrate to prevent lithium dendrite growth, Nat. Commun. 6 (2015) 7436 https://doi:10.1038/ncomms8436.